# Magnetic Resonance Separation Imaging Using a Divided Inversion Recovery Technique (DIRT)

James W. Goldfarb[1,2]*

**The divided inversion recovery technique is an MRI separation method based on tissue $T_1$ relaxation differences. When tissue $T_1$ relaxation times are longer than the time between inversion pulses in a segmented inversion recovery pulse sequence, longitudinal magnetization does not pass through the null point. Prior to additional inversion pulses, longitudinal magnetization may have an opposite polarity. Spatial displacement of tissues in inversion recovery balanced steady-state free-precession imaging has been shown to be due to this magnetization phase change resulting from incomplete magnetization recovery. In this paper, it is shown how this phase change can be used to provide image separation. A pulse sequence parameter, the time between inversion pulses (T180), can be adjusted to provide water-fat or fluid separation. Example water-fat and fluid separation images of the head, heart, and abdomen are presented. The water-fat separation performance was investigated by comparing image intensities in short-axis divided inversion recovery technique images of the heart. Fat, blood, and fluid signal was suppressed to the background noise level. Additionally, the separation performance was not affected by main magnetic field inhomogeneities. Magn Reson Med 63:1007–1014, 2010.**


**Key words: MRI; separation imaging; fat; lipid; fluid; myocardial infarction; pulse sequence; inversion recovery; bSSFP**

Tissue characterization in MRI is mostly performed using a visual assessment of image contrast generated by contrast agents or intrinsic magnetic relaxation time differences. MR images with pixel intensities weighted by $T_1$ or $T_2$ relaxation times are most commonly used. Additionally, preparation pulses can generate a variety of image contrasts between tissues. For example, fat saturation (1), magnetization transfer contrast radiofrequency pulses (2), or diffusion gradient pulses (3) may be added to impose specific image contrasts. The difference in pixel intensities allows identification of and discrimination between diseased and healthy tissues using a single image.

MR image separation techniques provide multiple images of the same imaging plane with pixels separated by an intrinsic tissue parameter. Water-fat separation (4) provides two images. Pixels composed primarily of lipids are displayed in the fat image and the other pixels composed primarily of water are displayed in the second image. Water-fat separation is most commonly performed using the chemical shift between water and fat nuclei. Image separation can also be performed using other parameters such as $T_1$ relaxation times or $T_1$-weighted imaging pixel intensity (5). In $T_1$-weighted spoiled gradient echo images, fat usually has the brightest signal and water-fat separation can be performed using a simple image intensity threshold.

Recently, an artifact was identified during late gadolinium-enhanced myocardial infarct imaging using an inversion recovery balanced steady-state free precession (IR-bSSFP) technique (6,7). This artifact is a spatial displacement of tissues and was shown to be due to a magnetization phase change resulting from incomplete magnetization recovery between subsequent inversions. This newly recognized IR-bSSFP imaging artifact is a result of the gradient refocusing and the reuse of magnetization. The phase change causes an image displacement of long $T_1$ species (cerebrospinal fluid and fluid-filled cysts). With specific imaging parameters (which are commonly used in late gadolinium-enhanced infarct imaging), long $T_1$ species are displaced in the phase-encoding dimension by half of the imaging field of view.

The purpose of this study was to further develop and evaluate an IR-bSSFP pulse sequence that exploits the change in polarity of longitudinal magnetization after inversion due to incomplete $T_1$ recovery. Such a sequence could provide tissue separation based on $T_1$ relaxation differences for a variety of tissue types such as fat and fluid.

## MATERIALS AND METHODS

### Theory and Technique Description

It has been reported that some structures appeared in wrong locations using an inversion recovery steady-state free precession imaging technique. Initially, it was reported that this artifact was caused by oscillations in the transient approach to steady state for regions with long $T_1$ relaxation times (6). It was later shown through computer simulations, phantom experiments, and human studies that this artifact is due to a change in phase from *k*-space segment to *k*-space segment of the detected magnetization from species with long $T_1$ relaxation times such as cysts, fluid collections, and cerebrospinal fluid (7). Depending on the number of *k*-space segments and view ordering, structures can be replicated throughout the image or displaced by half of the phase-encoding field of view.

[1]Department of Research and Education, Saint Francis Hospital, Roslyn, New York, USA.

[2]Program in Biomedical Engineering, SUNY Stony Brook, Stony Brook, New York, USA.

*Correspondence to: James W. Goldfarb, Ph.D.,Department of Research and Education, DeMatteis MRI, St. Francis Hospital, 100 Port Washington Boulevard, Roslyn, NY 11576. E-mail: james.goldfarb@chsli.org

Received 6 August 2009; revised 24 September 2009; accepted 13 October 2009.

DOI 10.1002/mrm.22281
Published online in Wiley InterScience (www.interscience.wiley.com).

This phenomenon was initially recognized as an image artifact. In this paper, I show how this phase change can be exploited to provide image separation based on $T_1$ relaxation times. Conventional MR images are reconstructed using matrices composed of rows acquired with different phase-encoding gradient amplitudes. To avoid significant image artifacts, the available signal or magnetization must be consistent or at least smoothly varying between neighboring rows or groups of rows (often called *k*-space segments) (8). This is often achieved by the use of "dummy" preparation pulses and/or collecting data in the so called steady-state, a period when available magnetization is essentially constant.

When MR pulse sequences with repetition times less than tissue $T_1$ relaxation times are used, longitudinal magnetization does not return to its equilibrium state and it is possible to have inconsistencies in the raw data matrix. One such case is bSSFP imaging (9). Magnetization is reused, yielding increased signal from long $T_1$ species. In the case of an inversion recovery sequence, if the $T_1$ relaxation time is much longer than the time between inversion pulses, the inverted longitudinal magnetization does not have a chance to pass through the null point, and longitudinal magnetization prior to additional inversion pulses may have an opposite polarity. If phase encoding is performed such that interleaving of *k*-space segments (odd and even *k*-space lines) is done prior to image reconstruction, species with long $T_1$ relaxation times will have an alternating phase in the raw data reconstruction matrix.

This is equivalent to multiplication by −1 on alternating rows of the raw data matrix (7). This *k*-space data multiplication is commonly used in MR image reconstruction (often called fft_shift, swapping, or chopping) and is equivalent to shifting the reconstructed image by half of the field of view. One should note that this only applies to long $T_1$ species as the magnetization of short $T_1$ species will have passed through the null point and have positive longitudinal magnetization in time periods between consecutive inversion pulses. I will see that the notion of "long" and "short" $T_1$ relaxation times is relative to an imaging parameter, T180, in the divided inversion recovery technique (DIRT) pulse sequence.

### DIRT Pulse Sequence (Segmented IR-bSSFP)

The cause of the displacement of long $T_1$ species in a segmented IR-bSSFP pulse sequence follows directly from the evolution of the magnetization during excitation and recovery (7). Figure 1 shows a schematic of the pulse sequence developed in this paper. The inversion recovery pulse sequence provides an image with two subimages divided in the middle based on $T_1$ relaxation times (Fig. 4) and will be called the DIRT.

One should note that the implemented DIRT pulse sequence uses three segments. Only one segment is necessary to generate an image with equivalent resolution of the separated images. The first segment is used for magnetization preparation. The second and third segments both collect *k*-space data matrices sufficiently sampled so that image aliasing does not occur. This effectively triples total acquisition time. Alternatively, the repeated *k*-space sampling in the third segment can be equivalently view as doubling the field of view and hence doubling acquisition time over that needed for unseparated image acquisition.

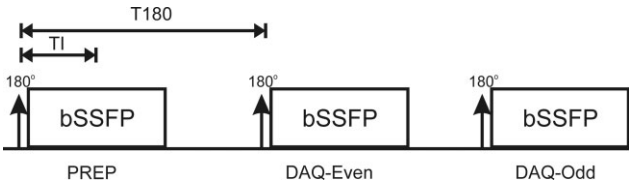


FIG. 1. Schematic diagram of the DIRT pulse sequence. A balanced steady-state free precession (bSSFP) refocused gradient-echo acquisition follows an inversion pulse (180°) and is repeated in three *k*-space segments. Data acquisition (DAQ) is performed in the second and third segments, where the even and odd *k*-space lines for image reconstruction are respectively collected. The first segment is used for magnetization preparation (PREP). TI = inversion time; T180 = time between inversion pulses.

### Computer Simulations

Bloch equation simulations of the longitudinal (Mz) and transverse magnetization (Mx) were performed to describe the DIRT technique and its characteristics over a range of delay times between inversion pulses (T180) at a field strength of 1.5 T. Simulation parameters were pulse repetition time = 2.4 ms; echo time = 1.5 ms; flip angle = 50°; a linear ramp of 10 radiofrequency pulses (10) was used for steady-state preparation; 128 radiofrequency pulses/*k*-space lines collected per segment, BW = 1180 Hz/pixel with linear filling of *k*-space. The tissues simulated were fat ($T_1$ = 260 ms; $T_2$ = 80 ms), blood ($T_1$ = 1.6 sec; $T_2$ = 200 ms), and fluid ($T_1$ = 4 sec; $T_2$ = 2 sec).

### Subjects

Eleven subjects participated in this study (nine men, two women; age 65.4 ± 10.9 years). Two healthy subjects underwent head imaging, six healthy subjects underwent heart imaging, two healthy subjects underwent spine and abdominal imaging, and one subject with known fat deposition (11–14) in a chronic myocardial infarction underwent heart imaging. The study of human subjects was approved by the institutional review board. All subjects signed an institutional review board–approved, Health Insurance Portability and Accountability Act–compliant consent form prior to study initiation.

### MRI

Imaging was performed using a 1.5-T clinical scanner (Siemens Magnetom Sonata, Erlangen, Germany), with gradients capable of 40 mT/m and 200 mT/m/ms. In vivo imaging sequence parameters were identical to those used for computer simulations (pulse repetition time/echo time/FA = 2.4/1.2/50; matrix = 256 × 512; voxel size = 2 × 1.8 × 8 mm; 128 phase-encoding lines per segment; interleaved segments; BW = 1180 Hz/pixel with linear filling of *k*-space; ECG synchronization, no averaging, T180 = one and two heartbeats

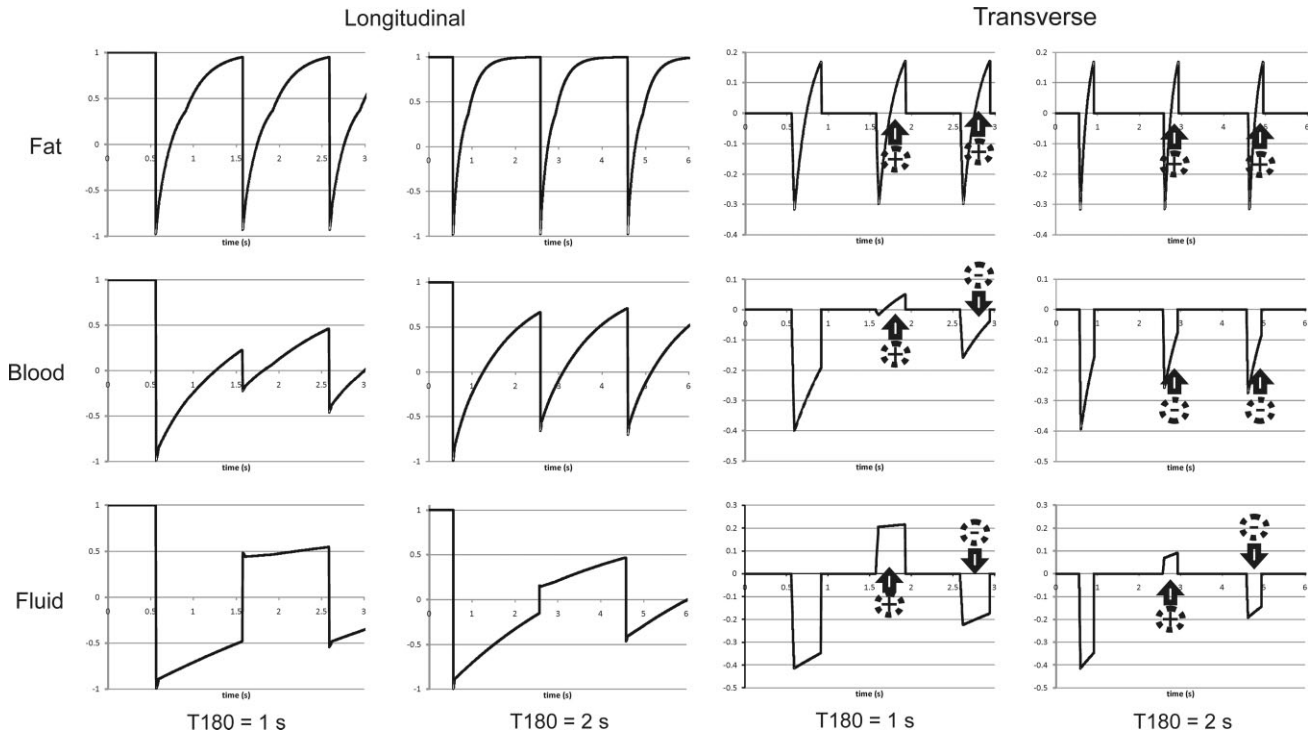


FIG. 2. Bloch equation simulation: longitudinal (Mz) and transverse magnetization (Mx) is shown for three tissue types and two settings of the T180 pulse sequence parameter. ± Signs with arrows show segments with positive and negative transverse magnetization at the *k*-space center. At the setting of T180 = 1 sec, fat has positive magnetization, while blood and fluid have alternating phases. At the setting of T180 = 2 sec, fat and blood both have consistent phase between segments, while fluid has an alternating phase. An alternating phase yields a spatial displacement after image reconstruction.

[approximately 1 and 2 sec]). Images were reconstructed on the scanner and the phase-encoding field of view was set such that it was twice the patient's size. Water-fat and fluid separation images were acquired to evaluate the technique in the head, heart, and abdomen. In six consecutive subjects, parallel short-axis slices from the base to the apex of the left ventricle were acquired to quantitatively evaluate the water-fat-fluid separation performance of the technique. The vendor's ECG gating was used in each case.

### Image and Statistical Analysis

Region-of-interest signal intensity (SI) measurements were made in the LV blood pool, epicardial fat, pericardial fluid, or cerebrospinal fluid and outside the body in the same locations in both water- and fat-separated short-axis heart images. The separation performance was evaluated by calculating the percentage SI change. The SI change for fat was calculated as:

$$100 \times (SI_{Tissue=Fat,\,Image=Fat}/SI_{Tissue=Fat,\,Image=Water})$$

and the SI change for water and fluid was calculated as:

$$100 \times (SI_{Tissue=Water\,or\,Fluid,\,Image=Water}/SI_{Tissue=Water\,or\,Fluid,\,Image=Fat}).$$

SIs of water, fat, fluid, and background noise in the water and fat images were compared using a two-tailed paired Student's *t* test to evaluate the quality of the technique's water-fat separation. Statistical analysis was performed using Analyze-It, version 2.11 (Analyze-It Ltd., Leeds, England). A value of $P \leq 0.05$ was considered to be significant.

## RESULTS

### Computer Simulations

Results from Bloch equation simulations (Fig. 2) showed marked changes dependent on tissue $T_1$ values of longitudinal and transverse magnetization in the DIRT technique. One can clearly see the change in longitudinal magnetization polarity (positive, negative, positive, negative) for fluid. Examination of the transverse magnetization shows the available signal for three tissues and two settings of the time between inversion pulses (T180). Note that there is always a marked recovery of magnetization during data acquisition resulting from the inversion pulse. This recovery is stronger for short $T_1$ species but still occurs for long $T_1$ species such as fluid.

Fat, as a result of its short $T_1$, has a consistent transverse magnetization in all three segments. Longer $T_1$ species such as blood and fluid have variable transverse magnetization. With T180 = 1 sec, both blood and fluid have alternating transverse magnetization phase during data acquisition. When the T180 time is increased to 2 sec, the behavior of blood is similar to that of fat (consistent segment-to-segment phase, although with a negative sign). With T180 = 2 sec, fluid retains its property of alternating

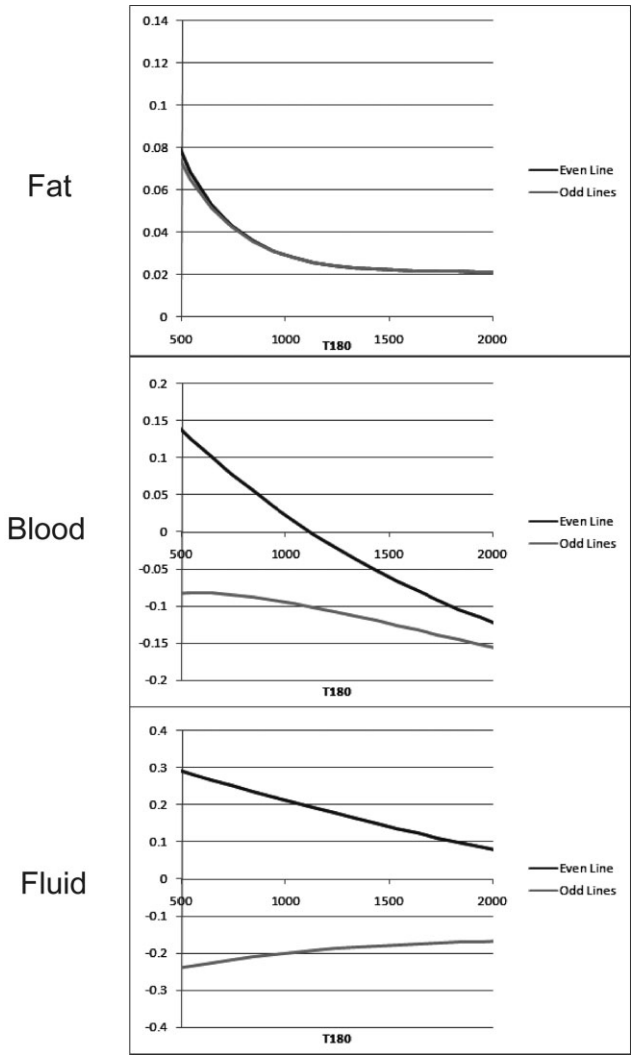


FIG. 3. Bloch equation simulation of the transverse magnetization (Mx) at the *k*-space center as a function of the time between inversion pulses (T180) for three tissue types. For the range of T180 times studied, the magnetization phase for the even and odd *k*-space lines of fat is always the same and conversely for fluid is always different. There is a phase transition of the even and odd- *k*-space lines for the transverse magnetization of blood. The phase is initially opposite and then transitions to the same phase.

phase. Note that alternating longitudinal polarity and transverse phase will yield spatial displacement and separation of tissues in the DIRT technique.

Simulations of the effects of increasing time between inversion pulses (T180) (Fig. 3) showed that the signal of fat remained essentially constant with the same phase in the even and odd *k*-space lines. For the range of T180 times studied, signal from fluid has an opposite phase in the even and odd *k*-space lines. On the other hand, the phase of the signal from blood changes as a function of T180. With short T180s, it has opposite phase, and with longer T180s, the same phase. A change in phase occurs at T180 = 1100 ms.

## In Vivo Experiments

High-quality images were obtained in all cases. Images displayed in Fig. 4 from a healthy volunteer show excellent fat and fluid separation. In DIRT fat-separation images, due to the alternating phase of transverse magnetization, blood, myocardium, pericardial fluid,

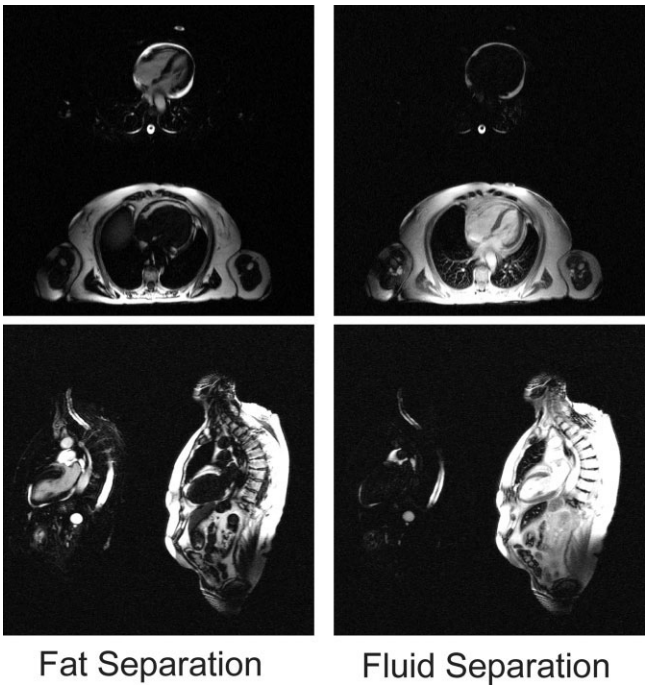


FIG. 4. Example DIRT images of a healthy volunteer in the four (top row) and two chamber (bottom row) orientations of the heart showing fat and fluid separation. Long $T_1$ species are displaced in the phase-encoding direction (upwards in four chamber images and to the left in two chamber images). In fat separation as a result of their relatively short $T_1$ relaxation times, fat structures are not displaced and remain in the bottom and right parts of the image. In fluid separation as a result of their relatively long $T_1$ relaxation times, fluid is displaced and is seen in the top and left parts of the image.

FIG. 5. Example thick slice projection DIRT images with fluid separation, showing pericardial fluid and an MR myelogram.

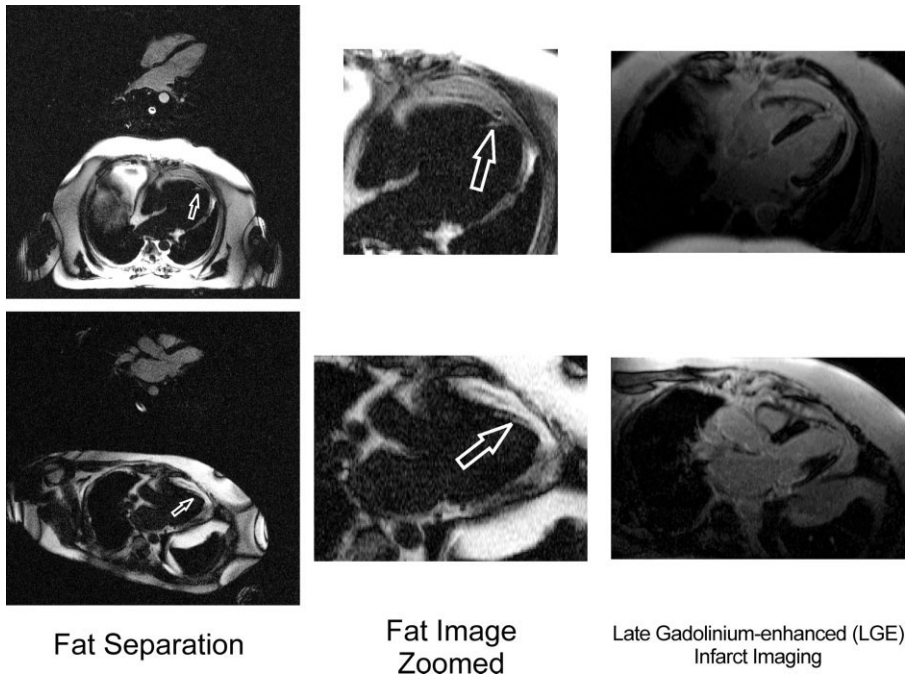


FIG. 6. Four- and three-chamber DIRT fat separation images of the heart, showing fatty deposition (arrows) of the apical myocardium in a patient with a chronic myocardial infarction. Late gadolinium-enhanced (LGE) images show the location of the apical infarct.

cerebrospinal fluid, and the gel from the ECG pad applied to the patient's chest are all displaced and fatty tissues of the body and arm are not displaced. In DIRT fluid-separation images, one can see pericardial fluid, cerebrospinal fluid, and a renal cyst displaced, while other tissues are not displaced. A thick slice with fluid separation shown in Fig. 5 shows the fluid around the heart and cerebrospinal fluid in the spine, resulting in an MR myelogram. Note the excellent water-fat separation at the edges of the field of view, in spite of severe magnetic field inhomogeneities and gradient field distortions, as evidenced by the banding artifacts and warping of the body.

In the patient with known fat deposition of a chronic myocardial infarct, DIRT fat separation clearly showed the fat deposition in the apex and apical septum of the left ventricle (Fig. 6). In DIRT fat-separation images, the blood and myocardial and cerebrospinal fluid tissues were displaced, clearly depicting the fat deposition in a myocardial segment with late gadolinium hyperenhancement. In another healthy volunteer with a renal cyst (Fig. 7, hollow arrows), fat and fluid separation perform well over a large field of view. A signal void (filled arrows) is also seen in the gallbladder, indicative of a large gallstone. An application of DIRT fluid separation in the head showed good separation of long $T_1$ species, including the eyes, cerebrospinal fluid in the ventricles, and sulci (Fig. 8).

### Quantitative Analysis

Representative short-axis water-fat–separated images are displayed in Fig. 9 and the graphical results of the quantitative region-of-interest analysis are displayed in Fig. 10 and tabulated in Tables 1 and 2. Water-fat separation performed well in all cases. Large percentage signal changes were seen when comparing the SIs in the water and fat images (Table 1). There was a significant difference in SIs of the same tissue type (fat, blood, fluid) between water and fat images (Table 2). There was not a significant difference between the background noise signal and the signal of the suppressed tissues (blood and fluid in the fat image and fat in the water image).

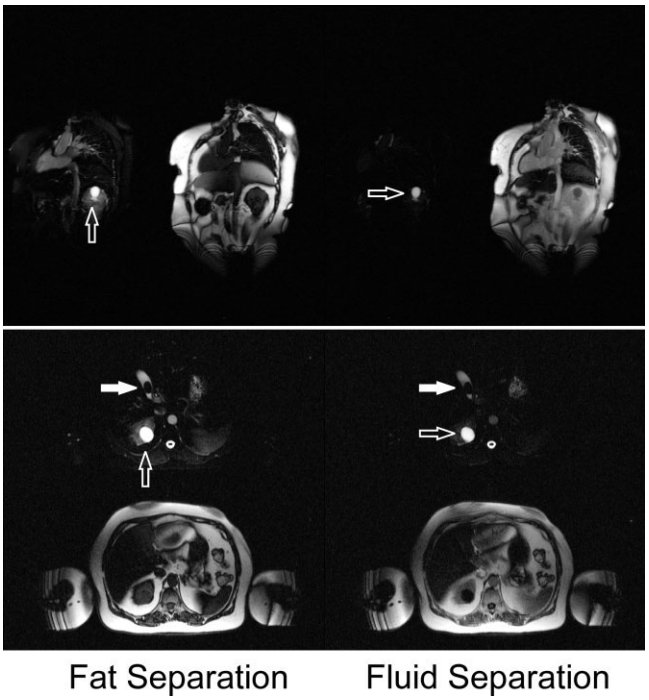


FIG. 7. Example images from a healthy volunteer showing fat and fluid separation using the DIRT technique. A smooth bordered mass is present in the right kidney (open arrows) and is displaced to the fluid only image, consistent with being a renal cyst. Also, a signal void is seen in the gallbladder (filled arrows), consistent with a gallstone.

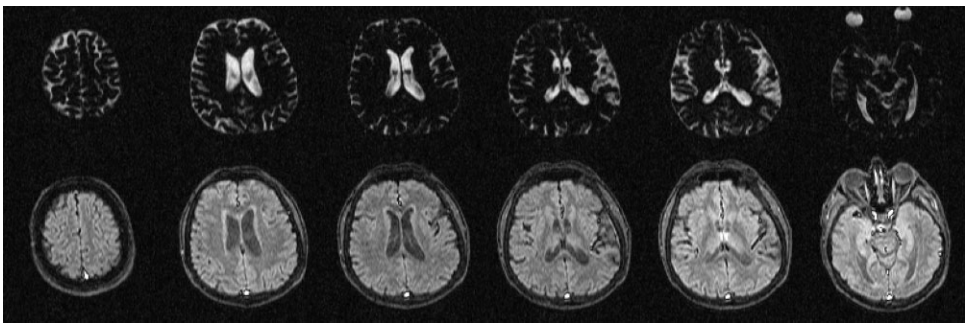

FIG. 8. Axial images of the head from a healthy volunteer, showing DIRT fluid separation.

## DISCUSSION

In this study, I have described, analyzed and presented initial results from a novel MRI method. The DIRT is based on a segmented IR-bSSFP pulse sequence. My results indicate the DIRT technique is an effective means of creating MR separation images based on tissue $T_1$ values. Water-fat separation and fluid separation are two straightforward applications of this technique. The technique is similar to the Dixon method, which utilizes different Larmour frequencies rather than $T_1$ relaxation times to alter the phases of target tissues (4).

There are numerous strategies, pulse sequences, and protocols for fat and fluid identification and quantitative analysis. Fat suppression using a chemically selective radiofrequency pulse is sensitive to main magnetic field inhomogeneities and difficult to apply to bSSFP imaging due to the continuous pulsing required to maintain a steady state (15,16). The DIRT technique utilizes the short $T_1$ of fatty tissues, as is commonly used in short inversion time recovery imaging (17), to provide water-fat separation and suppression. bSSFP images are typically acquired such that water and fat signals are 180° out of phase (18), resulting in a black line artifact. Pixels having signal contributions from both water and fat molecules will have signal cancellation and produce black line artifacts. The water-fat separation DIRT technique removed the black line artifact resulting from this opposed-phase signal cancellation. DIRT may find use as a fat saturation alternative for MR angiography and for the identification of lipid pathology such as lipomas and fatty infiltration of the right ventricle (19). Fluid or edema imaging is often performed using long echo time turbo-spin-echo imaging (20,21). The advantages of the DIRT technique can only be gleaned by direct comparison with existing techniques, which has not been performed in this paper. One advantage of DIRT separation (and MR separation methods in general) is that it provides not only suppressed hypointense tissue images (22) but also hyperintense tissue images of the suppressed species.

Since DIRT separation is based on $T_1$ values, the separation performance is not dependent on main magnetic field homogeneity. Banding image artifacts are still problematic in areas of magnetic field inhomogeneities because the current implementation is based on bSSFP imaging. There exist methods (23–27) compatible with DIRT separation to reduce and eliminate these artifacts, but they will extend imaging times due to the collection of multiple acquisitions.

There are several pulse sequence parameters in the DIRT technique that will affect both image contrast and separation. I have studied the T180 parameter and three tissue types. Adjustment of the time between inversion pulses (T180) changed the resulting separation. T180 = 1 sec consistently yielded water-fat separation and T180 = 2 sec consistently yielded fluid separation. I have not studied the effects of flip angle, number of *k*-space lines collected per segment, or the effects of recovery during data acquisition. Since the DIRT technique utilizes an inversion recovery pulse, images are inherently $T_1$ weighted. Other weightings may be added such as diffusion and $T_2$-preparation, but removal of the $T_1$-weighting component may not be possible.

In this paper, image reconstruction in the DIRT technique was performed on the MR scanner. The raw data matrix was constructed from odd and even *k*-space lines collected into two data acquisition segments. Image reconstruction was performed with a standard inverse Fourier transform. This provided a single image with two parts, short and long $T_1$ values. Alternatively, separate images can be reconstructed from the odd and even *k*-space lines and then the complex images can be added and subtracted to form equivalent short and long $T_1$-valued images. Images from the odd and even *k*-space lines may include additional information. This image

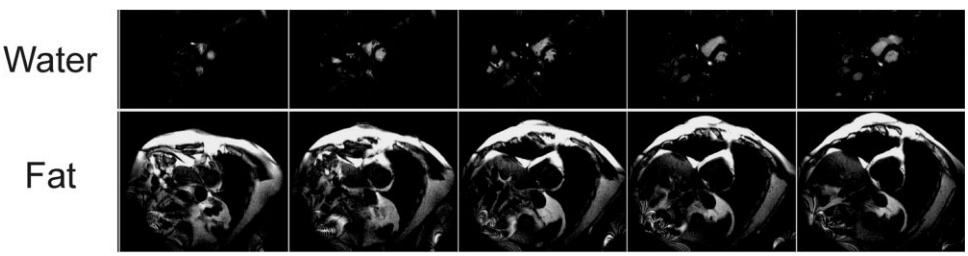


FIG. 9. Short-axis DIRT water-fat separation of the heart. Water-fat separation is achieved based on $T_1$ differences, rather than resonant frequency differences, and is therefore insensitive to magnetic field inhomogeneities.

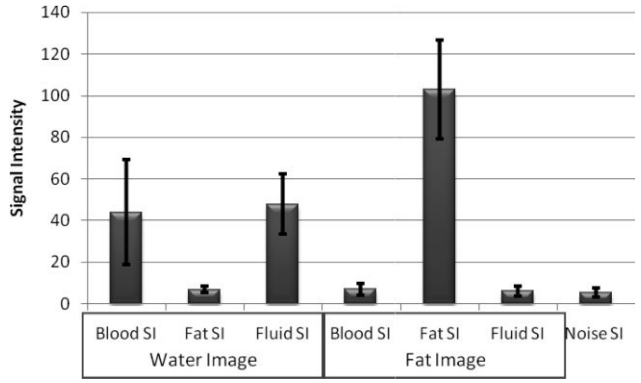


FIG. 10. Region-of-interest measurements from short-axis images of the heart showed that the fat SI was not significantly different from the noise in the water images, and fluid and blood SIs were not significantly different from the noise in the fat images ($P > 0.05$).

reconstruction process is similar to early water-fat separation techniques based on in- and opposed-phased imaging.

Often discussed and desired is the steady state obtained in "fast" MR pulse sequences. This steady state is a result of multiple radiofrequency pulses. In this paper, I have shown that there is another steady state in segmented pulse sequences. This would be a "segment" steady state where one would like to have the same signal in consecutive segments, rather than after consecutive radiofrequency pulses. The DIRT technique makes use of this change in magnetization in consecutive segments, specifically when there is a change in the polarity of longitudinal magnetization and resulting change in phase of the sampled transverse magnetization. One should note that one would like the magnitude of the magnetization to be equal in neighboring *k*-space lines. A change in magnitude will negatively affect separation performance.

In this paper, in vivo experiments were limited to T180 times of 1 and 2 sec. These settings came about naturally due to the use of cardiac gating in the pulse sequence. One second, with the pulse sequence triggered on every heartbeat, and 2 sec trigger on every other heartbeat with a resting heartbeat, without any MR gradient or radiofrequency pulsing. When cardiac gating is not required for imaging of the heart and blood vessels, the choice of T180 is flexible and could be further optimized.

Image separation methods have many applications (28–32). Identification of tissue types is simplified by identifying tissues in any single image rather than assessing relative contrast between neighboring tissues

Table 1
Percentage Signal Intensity Change: Comparing Water and Fat Images ($n = 6$)

| | Fat | Blood | Fluid |
|---|---|---|---|
| Mean ± SD | 1516.5 ± 115.3 | 665.28 ± 327.0 | 816.4 ± 222.4 |
| Minimum | 1414.1 | 316.9 | 520.6 |
| Maximum | 1677.3 | 1062.6 | 1179.4 |

Table 2
*P* Values From Student *t* Test Comparing SI in DIRT Water-Fat–Separated Images ($n = 6$)

| | | Water image | | | |
|---|---|---|---|---|---|
| | | Fat | Blood | Fluid | Noise |
| Fat image | Fat | <0.001 | | | |
| | Blood | | 0.014 | | 0.068 |
| | Fluid | | | <0.001 | 0.522 |
| | Noise | 0.169 | | | |

in images weighted by intrinsic MR parameters such as $T_1$, $T_2$, or spin density. Separation methods provide images that can be efficiently processed with simple thresholding algorithms to measure object two-dimensional areas or three-dimensional volumes. Application of parallel imaging techniques (33,34) could be performed to improve the shortest possible inversion time with prescan, self-calibration, or calibration collected from the first inversion segment where no data acquisition has been used.

I have not investigated many limitations of the proposed technique. This includes the limitations of $T_1$ relaxation separation. The method performed well for separating relatively short and long $T_1$ species. I have not demonstrated that smaller $T_1$ differences can be separated, such as between gray and white matter in the brain or viable and nonviable myocardium in late gadolinium-enhanced infarct imaging. This may be possible, but is beyond the current initial study. The blurring due to effective addition and subtraction of images with different point spread functions has not been studied. Point spread functions for inversion recovery single-shot pulse sequences are often complicated by the fact that nulling a broad range of high spatial frequencies is difficult due to magnetization regrowth during data acquisition. Remnant ghost could be problematic for midrange $T_1$ relaxation times and was not studied in this paper. Subjects were studied with normal heart rhythms and R-R intervals in the range of 900-1100 ms. This allowed the setting of the T180 parameter to be the R-R interval. This may be problematic in patients with arrhythmias, tachycardia, or bradycardia.

## CONCLUSIONS

Separation and identification of tissues based on their $T_1$ relaxation times can be achieved using a segmented IR-bSSFP pulse sequence. Tissue separation is achieved as a result of a phase change of the transverse magnetization resulting from incomplete magnetization recovery of relatively long $T_1$ target tissues following in inversion pulse. Fat and fluid separation are two feasible applications of the DIRT technique.

## REFERENCES

1. Rosen BR, Wedeen VJ, Brady TJ. Selective saturation NMR imaging. J Comput Assist Tomogr 1984;8:813–818.
2. Wolff SD, Balaban RS. Magnetization transfer contrast (MTC) and tissue water proton relaxation in vivo. Magn Reson Med 1989;10: 135–144.

3. Hagmann P, Jonasson L, Maeder P, Thiran JP, Wedeen VJ, Meuli R. Understanding diffusion MR imaging techniques: from scalar diffusion-weighted imaging to diffusion tensor imaging and beyond. Radiographics 2006;26(suppl 1):S205–223.
4. Ma J. Dixon techniques for water and fat imaging. J Magn Reson Imaging 2008;28:543–558.
5. Jacob AN, Adams-Huet B, Raskin P. The visceral and subcutaneous fat changes in type 1 diabetes: a pilot study. Diabetes Obes Metab 2006;8:524–530.
6. Kellman P, Dyke CK, Aletras AH, McVeigh ER, Arai AE. Artifact suppression in imaging of myocardial infarction using B1-weighted phased-array combined phase-sensitive inversion recovery. Magn Reson Med 2004;51:408–412.
7. Goldfarb JW, Arnold S, Schapiro W, Reichek N. On the cause of spatial displacement of long T1 species in segmented inversion recovery prepared imaging. Magn Reson Med 2005;54:481–485.
8. Atkinson DJ, Edelman RR. Cineangiography of the heart in a single breath hold with a segmented turboFLASH sequence. Radiology 1991;178:357–360.
9. Oppelt A, Graumann R, Barfuss H, Fischer H, Hartl W, Schajor W. FISP – a new fast MRI sequence. Eclectromedia 1986;54:15–18.
10. Deshpande VS, Chung YC, Zhang Q, Shea SM, Li D. Reduction of transient signal oscillations in true-FISP using a linear flip angle series magnetization preparation. Magn Reson Med 2003;49:151–157.
11. Baroldi G, Silver MD, De Maria R, Parodi O, Pellegrini A. Lipomatous metaplasia in left ventricular scar. Can J Cardiol 1997;13:65–71.
12. Goldfarb JW. Fat-water separated delayed hyperenhanced myocardial infarct imaging. Magn Reson Med 2008;60:503–509.
13. Goldfarb JW, Arnold S, Roth M, Han J. T1-weighted magnetic resonance imaging shows fatty deposition after myocardial infarction. Magn Reson Med 2007;57:828–834.
14. Su L, Siegel JE, Fishbein MC. Adipose tissue in myocardial infarction. Cardiovasc Pathol 2004;13:98–102.
15. Nguyen TD, Spincemaille P, Wang Y. Improved magnetization preparation for navigator steady-state free precession 3D coronary MR angiography. Magn Reson Med 2004;51:1297–1300.
16. Scheffler K, Heid O, Hennig J. Magnetization preparation during the steady state: fat-saturated 3D TrueFISP. Magn Reson Med 2001;45:1075–1080.
17. Bydder GM, Steiner RE, Blumgart LH, Khenia S, Young IR. MR imaging of the liver using short TI inversion recovery sequences. J Comput Assist Tomogr 1985;9:1084–1089.
18. Hargreaves BA, Vasanawala SS, Nayak KS, Hu BS, Nishimura DG. Fat-suppressed steady-state free precession imaging using phase detection. Magn Reson Med 2003;50:210–213.
19. Burke AP, Farb A, Tashko G, Virmani R. Arrhythmogenic right ventricular cardiomyopathy and fatty replacement of the right ventricular myocardium: are they different diseases? Circulation 1998;97:1571–1580.
20. Abdel-Aty H, Simonetti O, Friedrich MG. T2-weighted cardiovascular magnetic resonance imaging. J Magn Reson Imaging 2007;26:452–459.
21. Reinbold C, Bret PM, Guibaud L, Barkun AN, Genin G, Atri M. MR cholangiopancreatography: potential clinical applications. Radiographics 1996;16:309–320.
22. Bangerter NK, Hargreaves BA, Gold GE, Stucker DT, Nishimura DG. Fluid-attenuated inversion-recovery SSFP imaging. J Magn Reson Imaging 2006;24:1426–1431.
23. Foxall DL. Frequency-modulated steady-state free precession imaging. Magn Reson Med 2002;48:502–508.
24. Cukur T, Lustig M, Nishimura DG. Multiple-profile homogeneous image combination: application to phase-cycled SSFP and multicoil imaging. Magn Reson Med 2008;60:732–738.
25. Cukur T, Nishimura DG. Multiple repetition time balanced steady-state free precession imaging. Magn Reson Med 2009;62:193–204.
26. Elliott AM, Bernstein MA, Ward HA, Lane J, Witte RJ. Nonlinear averaging reconstruction method for phase-cycle SSFP. Magn Reson Imaging 2007;25:359–364.
27. Nayak KS, Lee HL, Hargreaves BA, Hu BS. Wideband SSFP: alternating repetition time balanced steady state free precession with increased band spacing. Magn Reson Med 2007;58:931–938.
28. Costa DN, Pedrosa I, McKenzie C, Reeder SB, Rofsky NM. Body MRI using IDEAL. AJR Am J Roentgenol 2008;190:1076–1084.
29. Gerdes CM, Kijowski R, Reeder SB. IDEAL imaging of the musculoskeletal system: robust water fat separation for uniform fat suppression, marrow evaluation, and cartilage imaging. AJR Am J Roentgenol 2007;189:W284–291.
30. Gold GE, Reeder SB, Yu H, Kornaat P, Shimakawa AS, Johnson JW, Pelc NJ, Beaulieu CF, Brittain JH. Articular cartilage of the knee: rapid three-dimensional MR imaging at 3.0 T with IDEAL balanced steady-state free precession—initial experience. Radiology 2006;240:546–551.
31. Reeder SB, Markl M, Yu H, Hellinger JC, Herfkens RJ, Pelc NJ. Cardiac CINE imaging with IDEAL water-fat separation and steady-state free precession. J Magn Reson Imaging 2005;22:44–52.
32. Reeder SB, Yu H, Johnson JW, Shimakawa A, Brittain JH, Pelc NJ, Beaulieu CF, Gold GE. T1- and T2-weighted fast spin-echo imaging of the brachial plexus and cervical spine with IDEAL water-fat separation. J Magn Reson Imaging 2006;24:825–832.
33. Griswold MA, Jakob PM, Heidemann RM, Nittka M, Jellus V, Wang J, Kiefer B, Haase A. Generalized autocalibrating partially parallel acquisitions (GRAPPA). Magn Reson Med 2002;47:1202–1210.
34. Pruessmann KP, Weiger M, Scheidegger MB, Boesiger P. SENSE: sensitivity encoding for fast MRI. Magn Reson Med 1999;42:952–962.